A Combined Experimental and Theoretical Study of RuO_2/TiO_2 Heterostructures as a Photoelectrocatalyst for Hydrogen Evolution

Supporting Information

Mohammad Kaikhosravi[a] *, Hassan Hadadzadeh*[a*], *Hossein Farrokhpour*[a], *Abdollah Salimi*[b], *Hamed Mohtasham*[b], *Annette Foelske*[c], *and Markus Sauer*[c]

[a] Department of Chemistry, Isfahan University of Technology, Isfahan 84156-83111, Iran

[b] Department of Chemistry, University of Kurdistan, Sanandaj 66177-15175, Iran

[c] Analytical Instrumentation Center, TU Wien, Lehargasse 6, 1060 Vienna, Austria

* **Corresponding Author:** Hassan Hadadzadeh, Email: hadad@iut.ac.ir

Twenty pages (page S1-page S20) and nineteen figures (Figure S1-S19).

Synthesis route for the preparation of $Na_2[Ti(C_2O_4)_3]$

$TiCl_4$ (1.75 g, 0.001 mol, 1 eq), $Na_2C_2O_4$ (0.54 g, 0.004 mol, 3.7 eq), and $AgNO_3$ (0.68 g, 0.004 mol, 4 eq) were suspended in dried acetone (10 mL) and stirred in a flask covered with a black paper for 1 h. The silver chloride (AgCl) precipitated was centrifuged off and then anhydrous ether was added to precipitate the crude product. The obtain precipitate was recrystallized from ethanol. (Yield: ca. 70%)

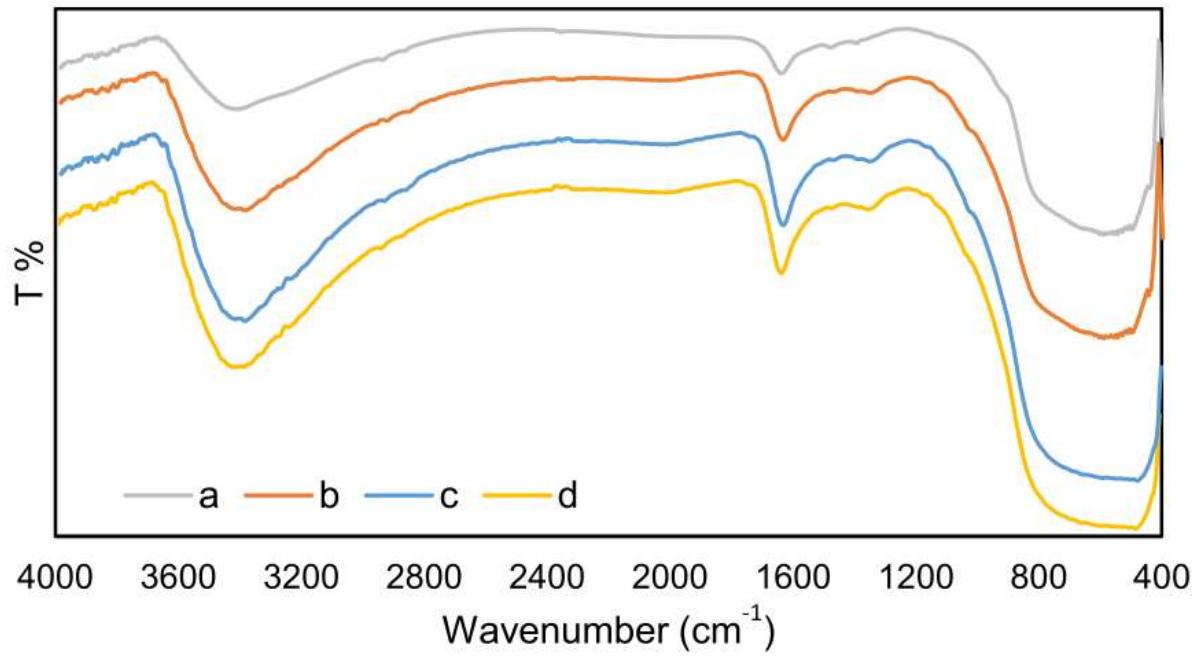

Figure S1: FTIR spectra of the TiO_2 samples calcined at various temperatures (a: 400 °C, b: 500 °C, and c: 600 °C), and d: 8 wt % RuO_2/TiO_2) heterostructure.

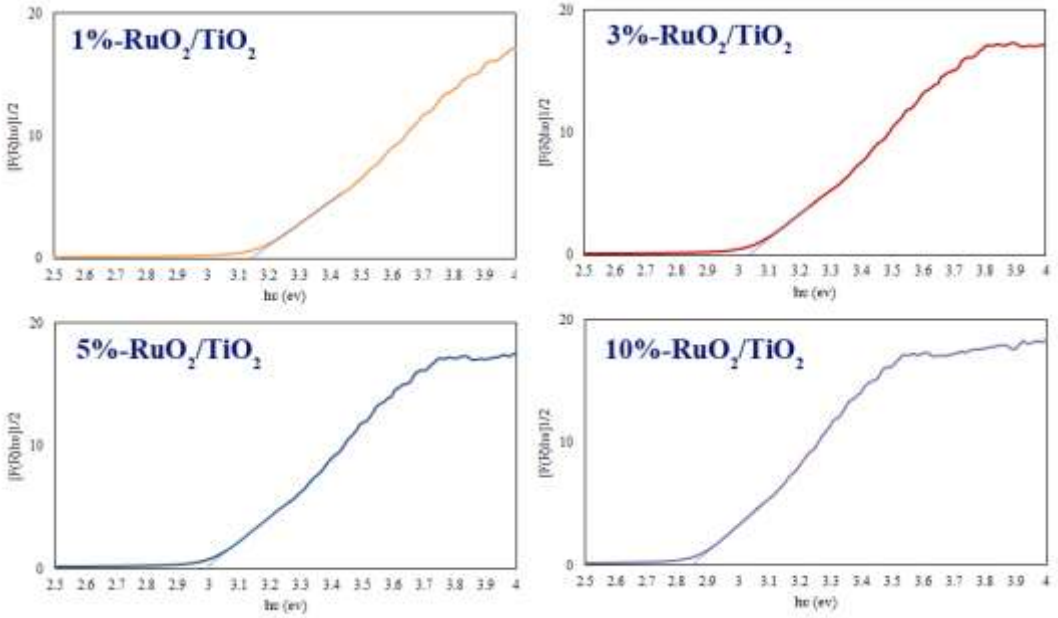

Figure S2: Band gaps of the RuO_2/TiO_2 heterostructures calculated by converting the reflectance to the absorption values by the utilization of the Kubelka-Munk algorithm.

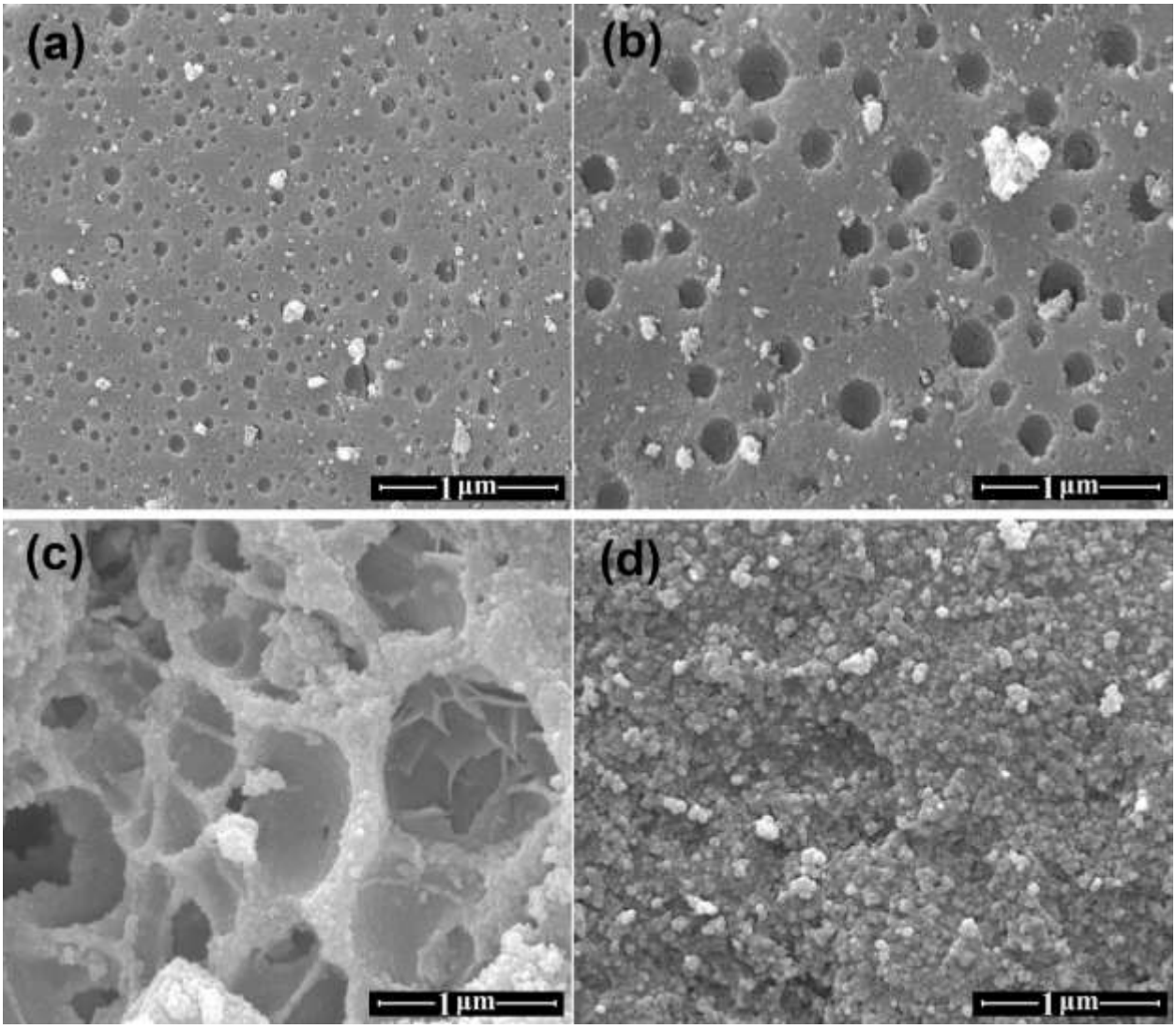

Figure S3: FESEM images of the mesoporous TiO_2 (a, b, and c prepared at 400, 500, and 600 °C, respectively), and 8 wt % RuO_2/TiO_2 heterostructure.

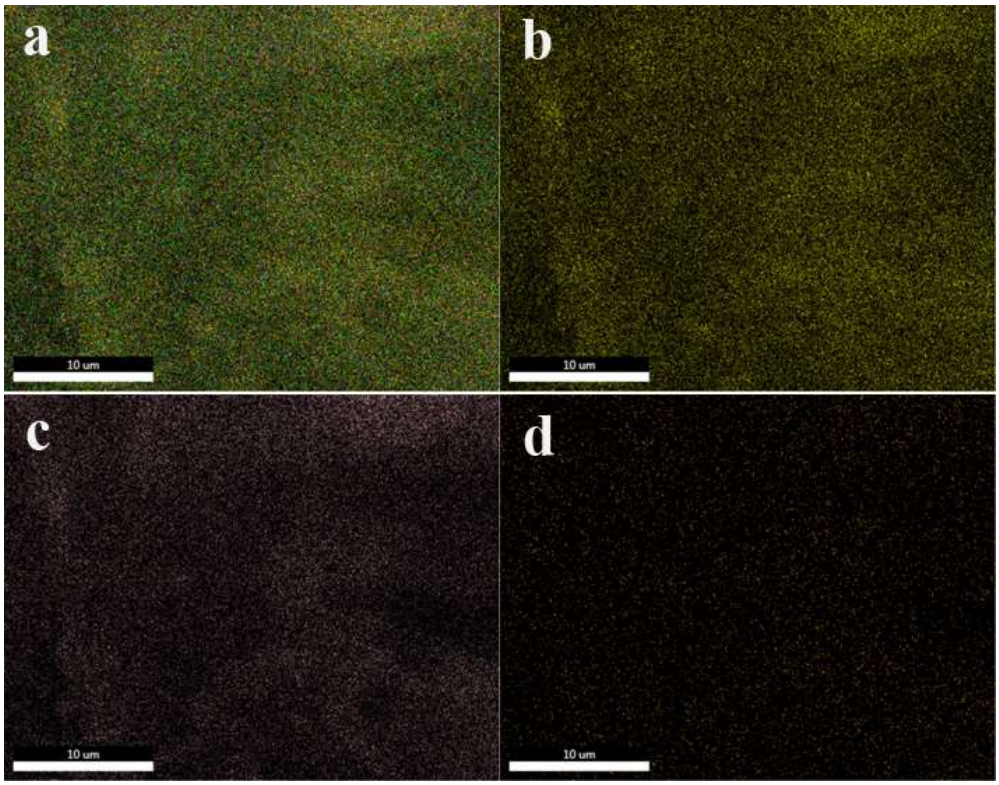

Figure S4: Elemental mappings of 8 wt % RuO_2/TiO_2 heterostructure, (a) all elements, (b) titanium, (c) oxygen, and (d) ruthenium.

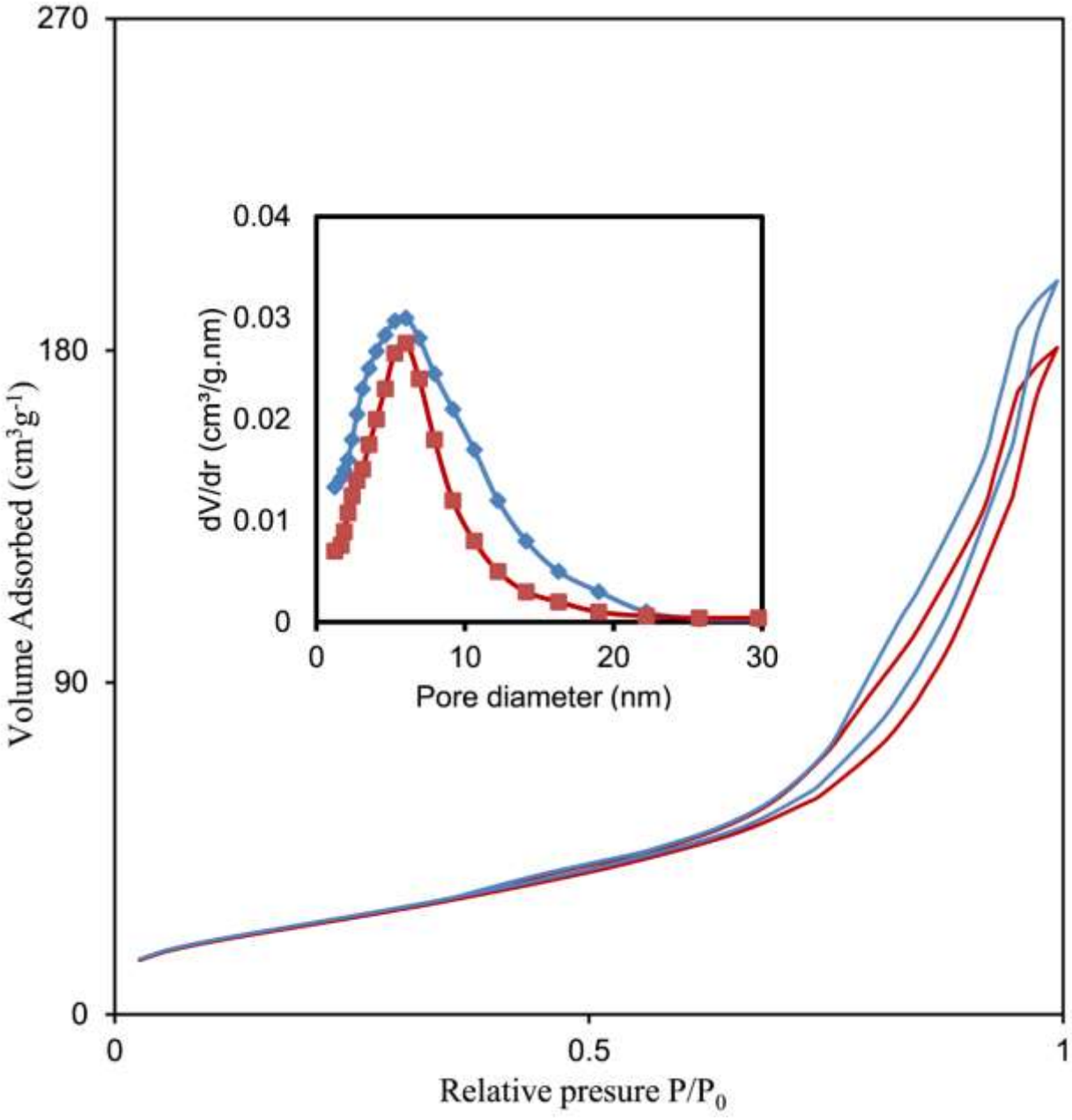

Figure S5. Nitrogen adsorption−desorption isotherms and the corresponding pore size distributions (inset) of the pure TiO_2 (red) and 8 wt % RuO_2/TiO_2 (blue) photoelectrocatalyst.

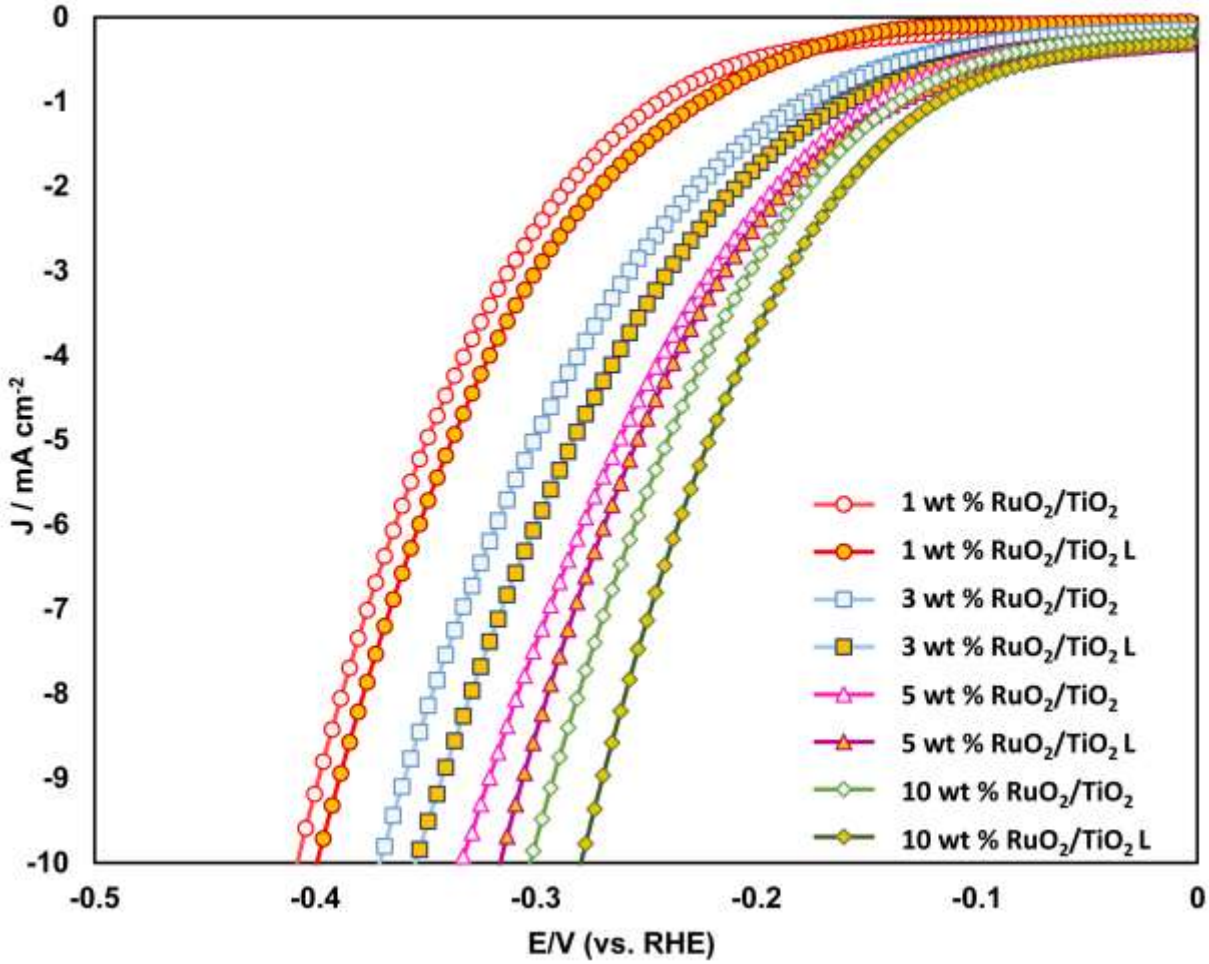

Figure S6: Linear sweep voltammograms of RuO_2/TiO_2 heterostructures towards HER under dark and light conditions.

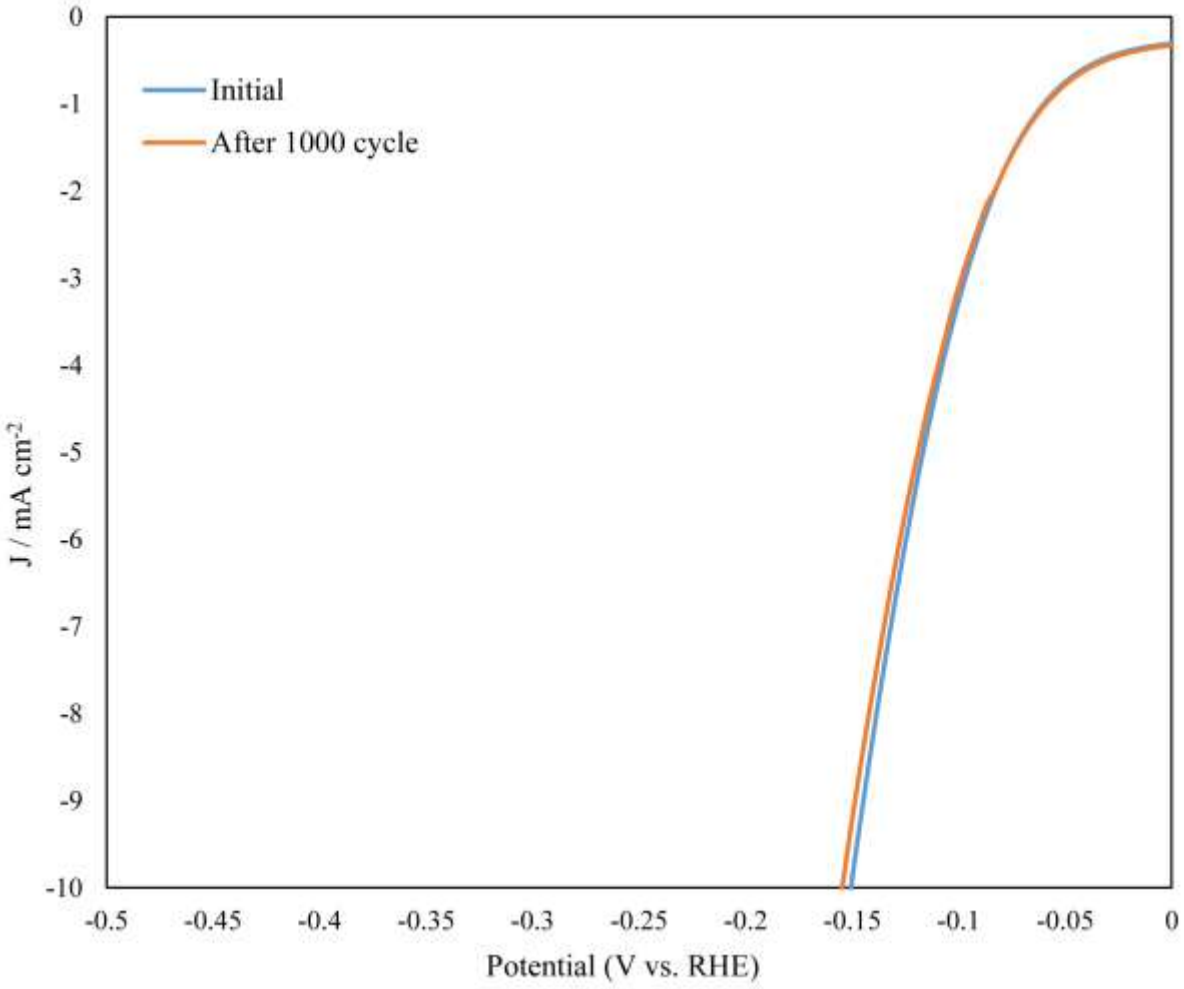

Figure S7: Linear sweep voltammograms of the 8 wt % RuO_2/TiO_2 heterostructure towards HER before and after 1000 potential cycles.

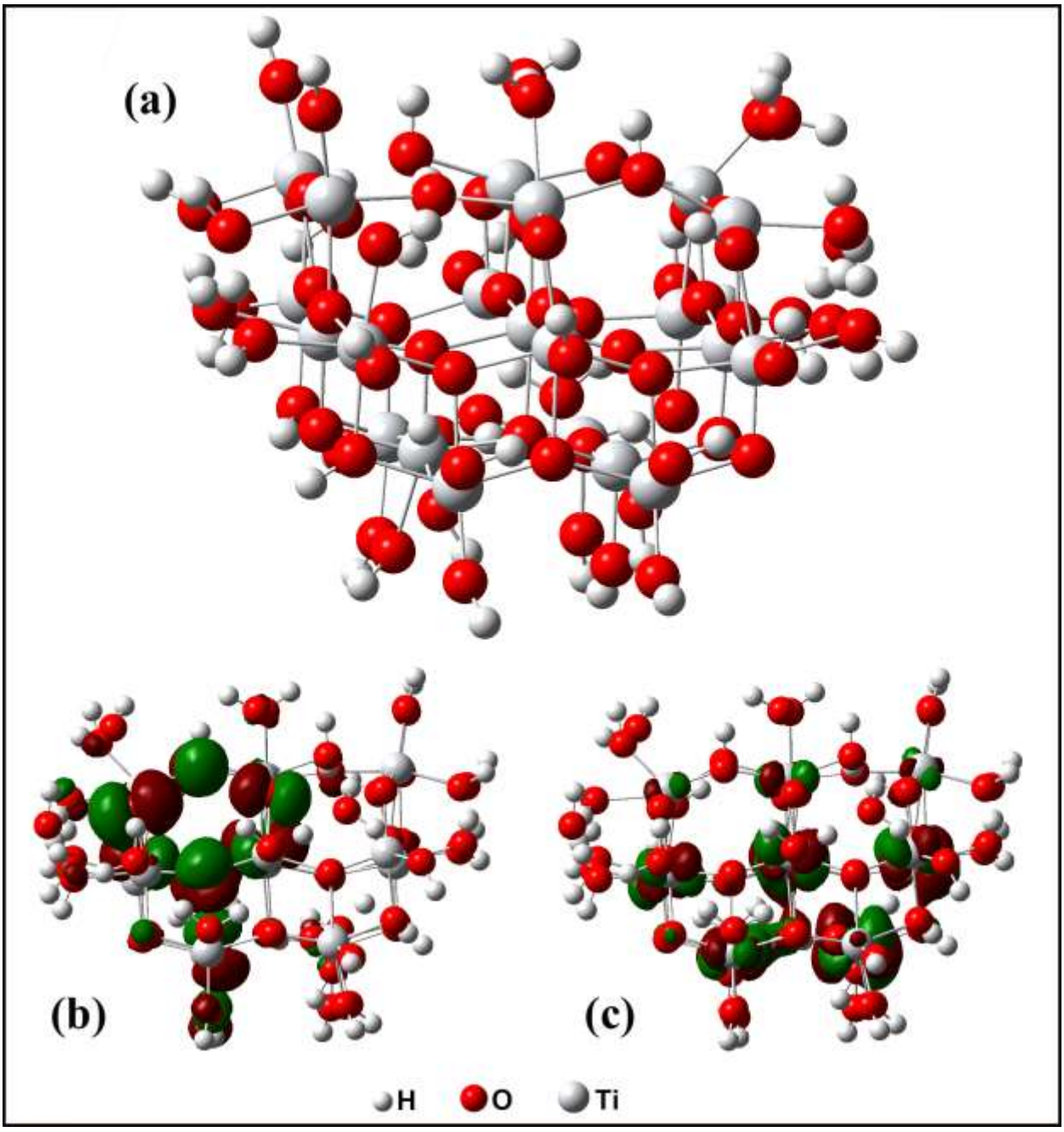

Figure S8: Optimized TiO_2 Clusters (a), HOMO (b), and LUMO (c).

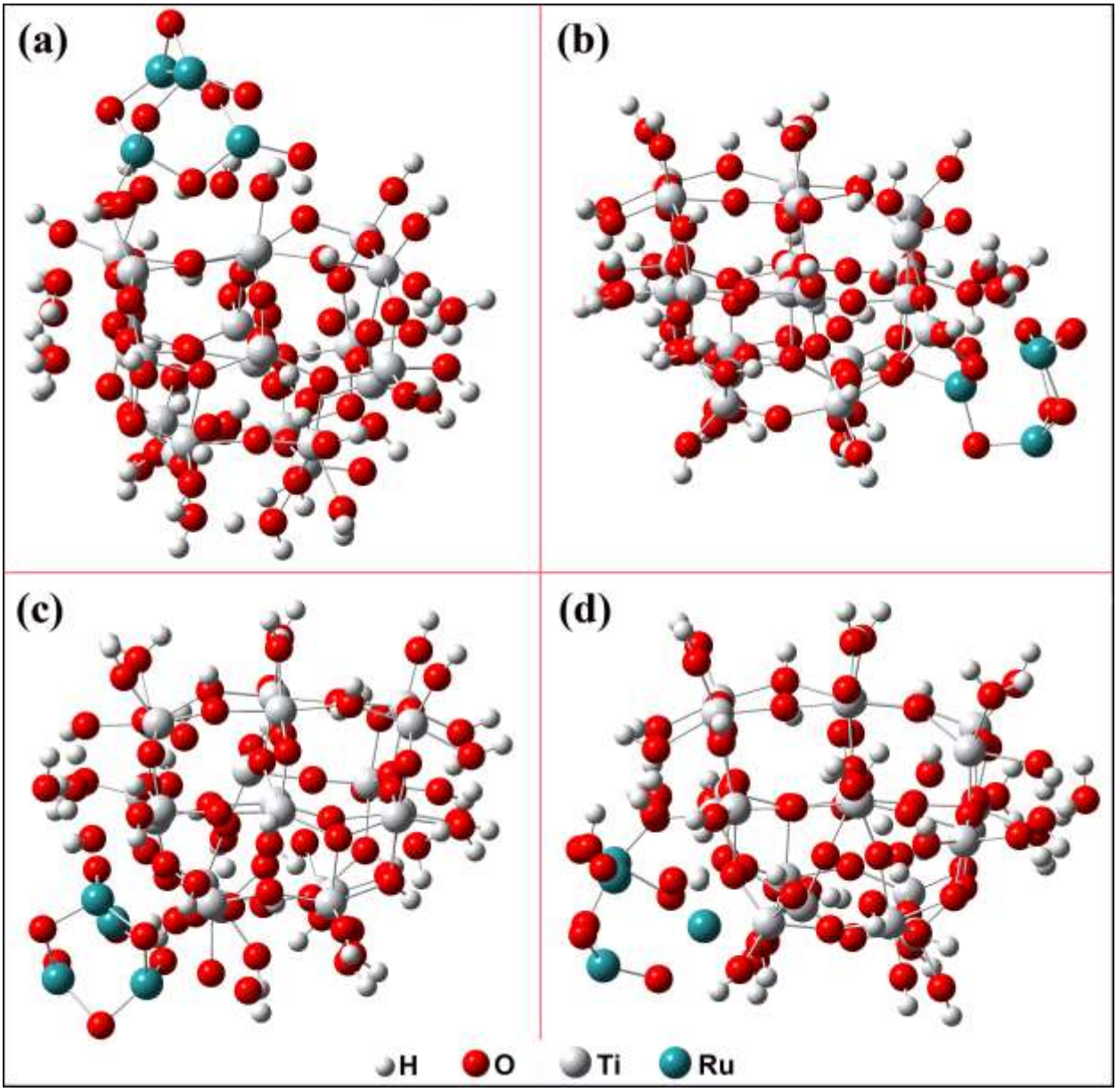

Figure S9: Optimized RuO_2/TiO_2 clusters in different orientations.

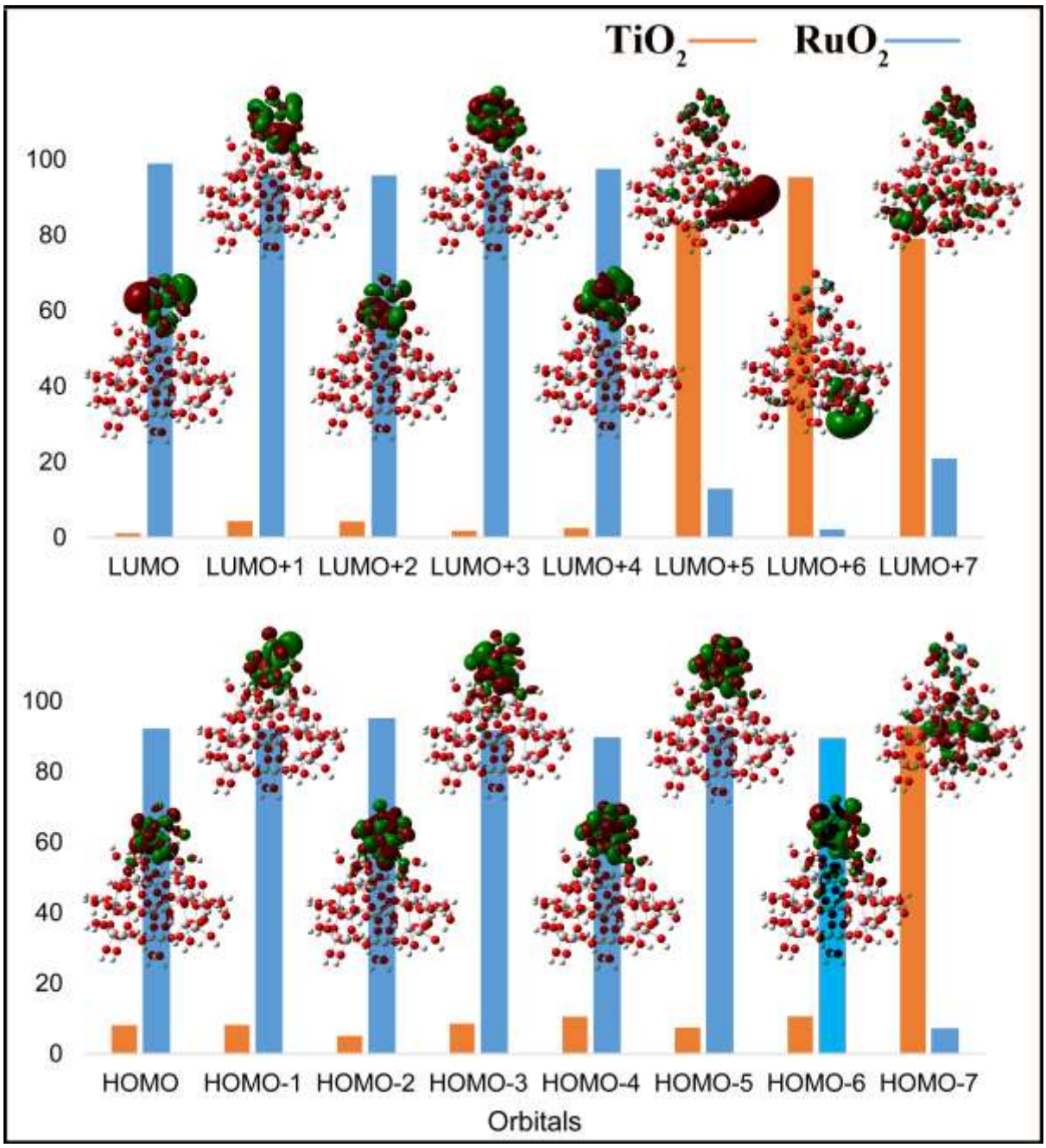

Figure S10: Several occupied and unoccupied molecular orbitals (HOMO-7 to LUMO+7) and fragments contributions in RuO_2/TiO_2 cluster **a**.

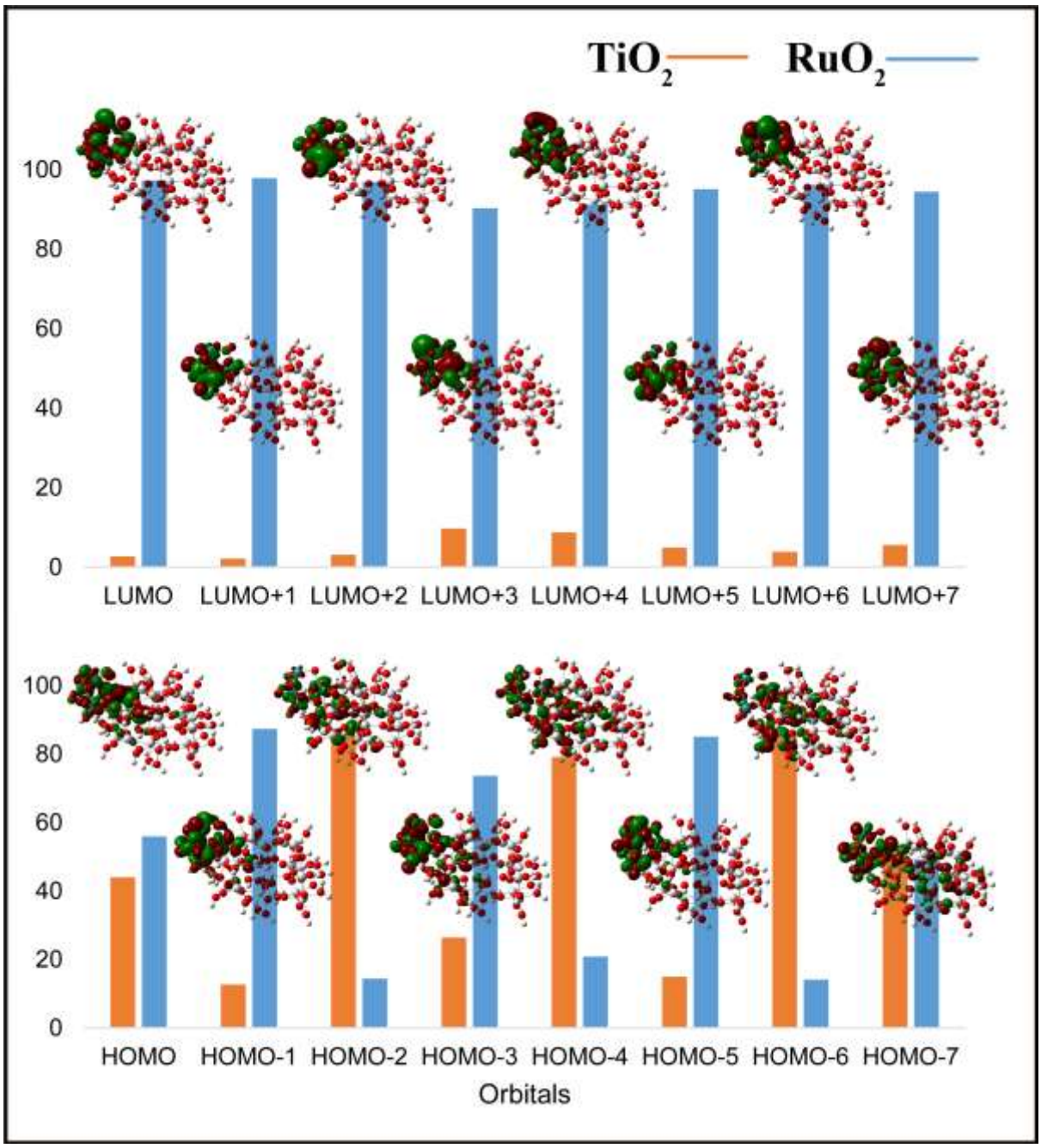

Figure S11: Several occupied and unoccupied molecular orbitals (HOMO-7 to LUMO+7) and fragments contributions in RuO_2/TiO_2 cluster **b**

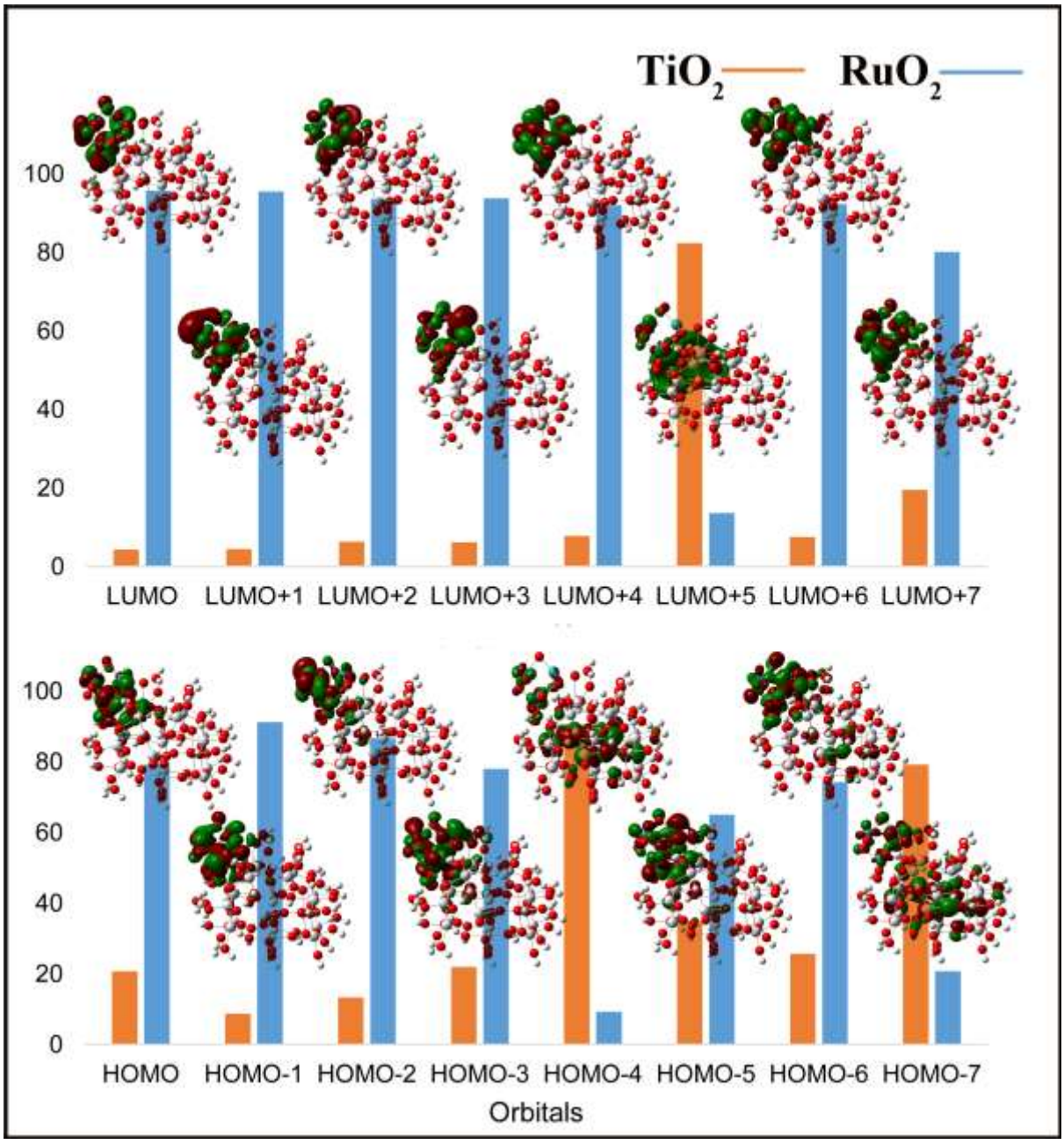

Figure S12: Several occupied and unoccupied molecular orbitals (HOMO-7 to LUMO+7) and fragment contributions in RuO_2/TiO_2 cluster **c**

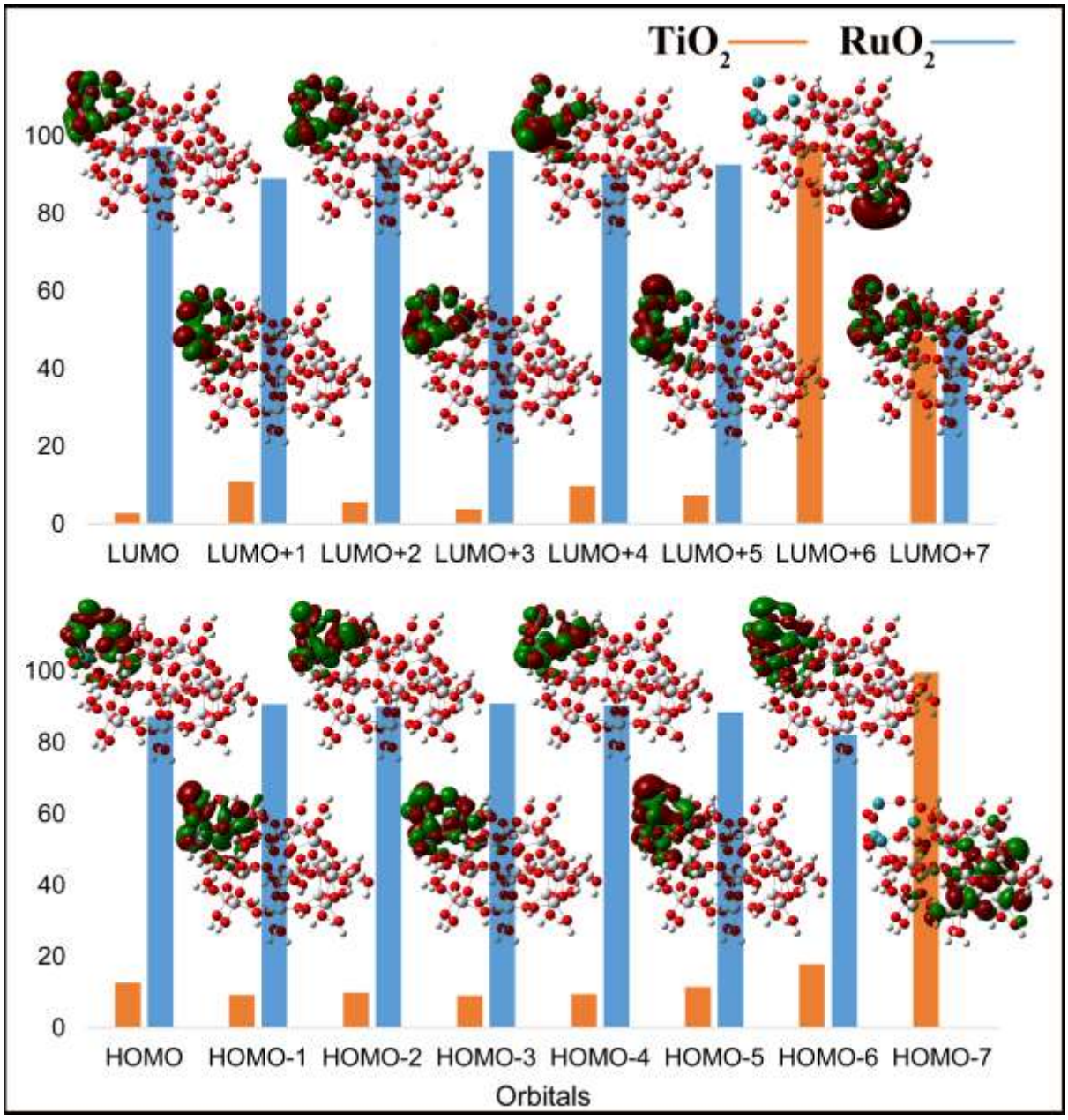

Figure S13: Several occupied and unoccupied molecular orbitals (HOMO-7 to LUMO+7) and fragment contributions in RuO_2/TiO_2 cluster **d**.

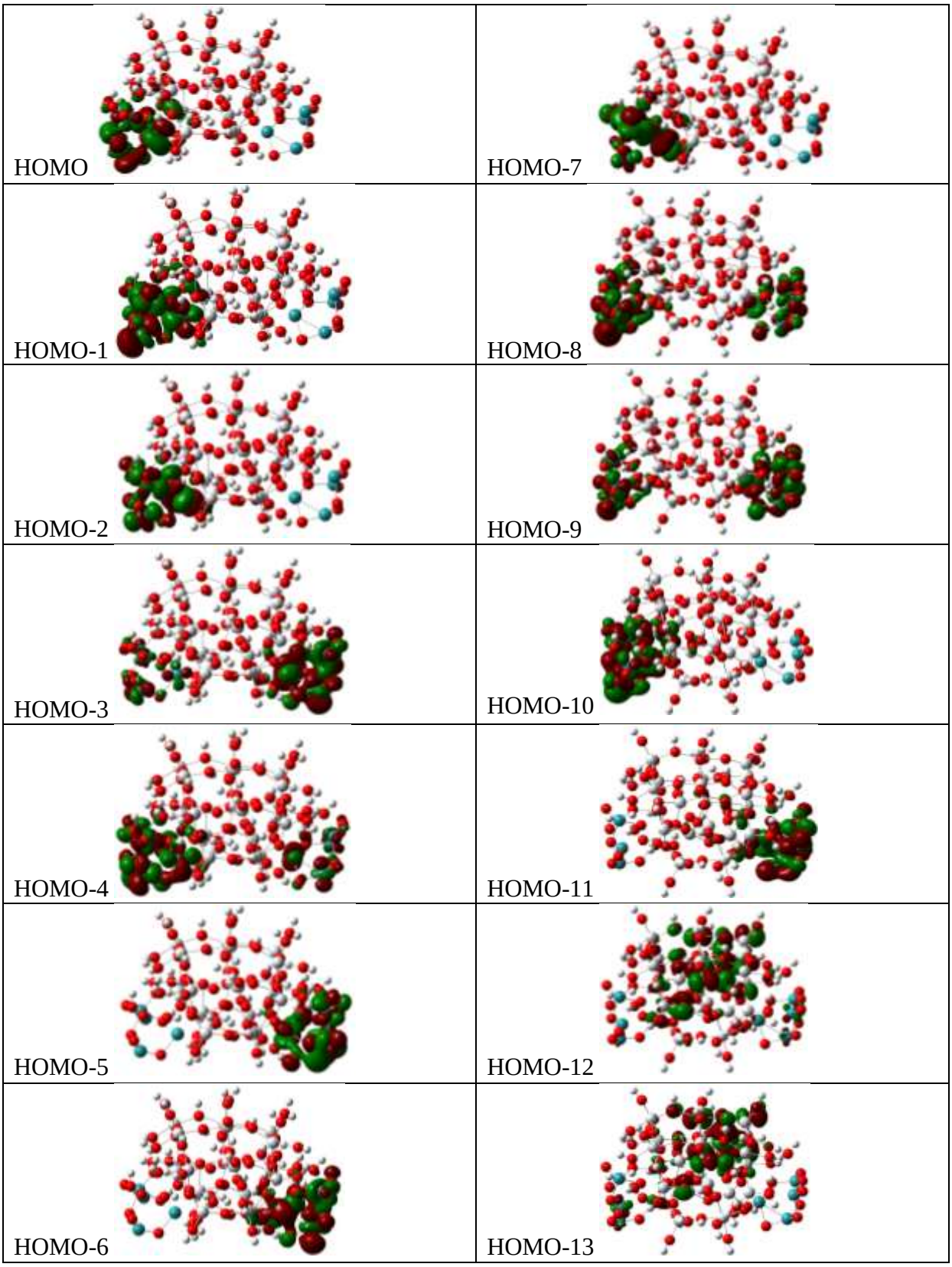

Figure S14: Occupied molecular orbitals (HOMO to HOMO-13) of cluster **e**.

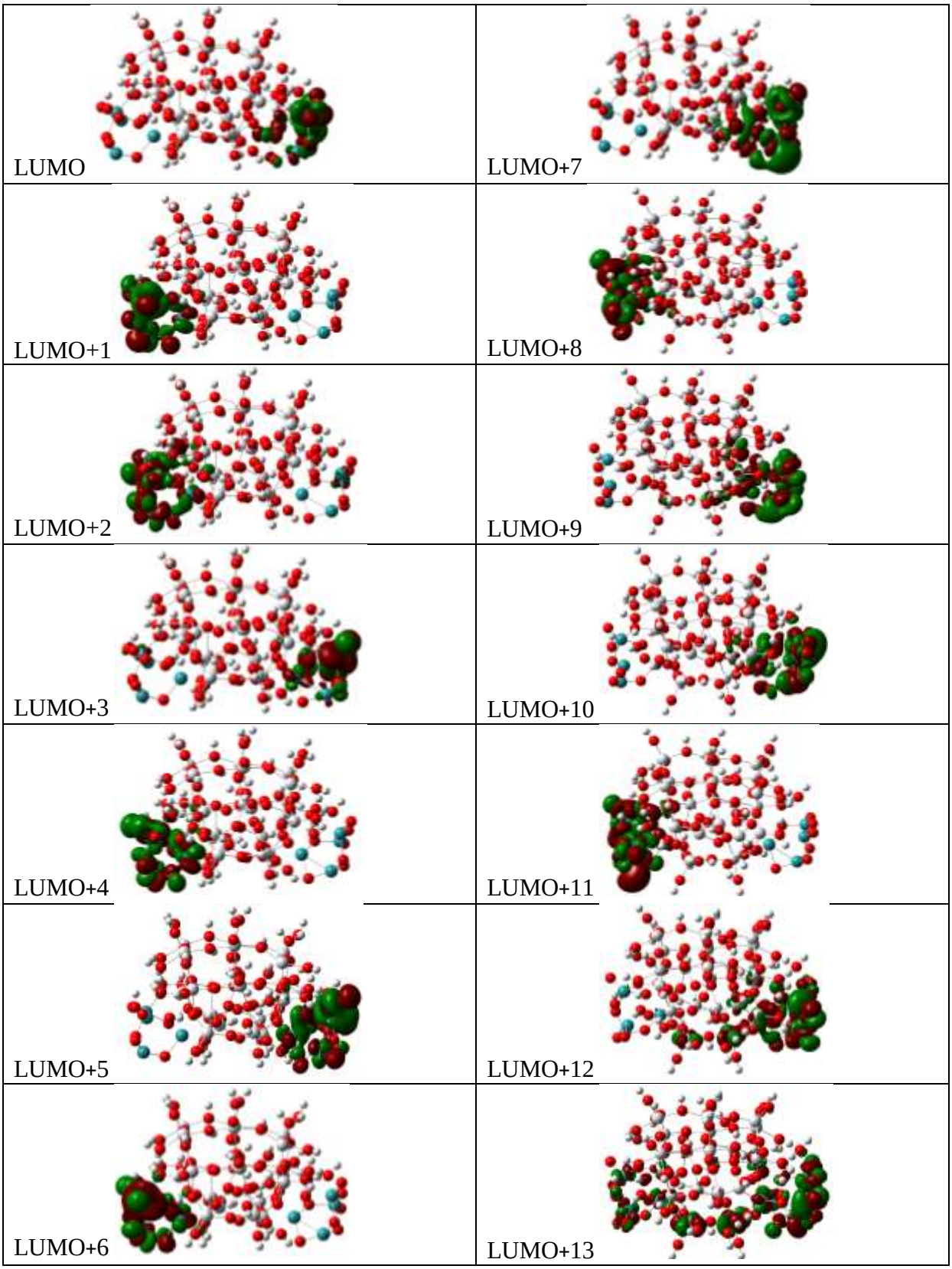

Figure S15: Unoccupied molecular orbitals (LUMO to LUMO+13) of cluster **e**.

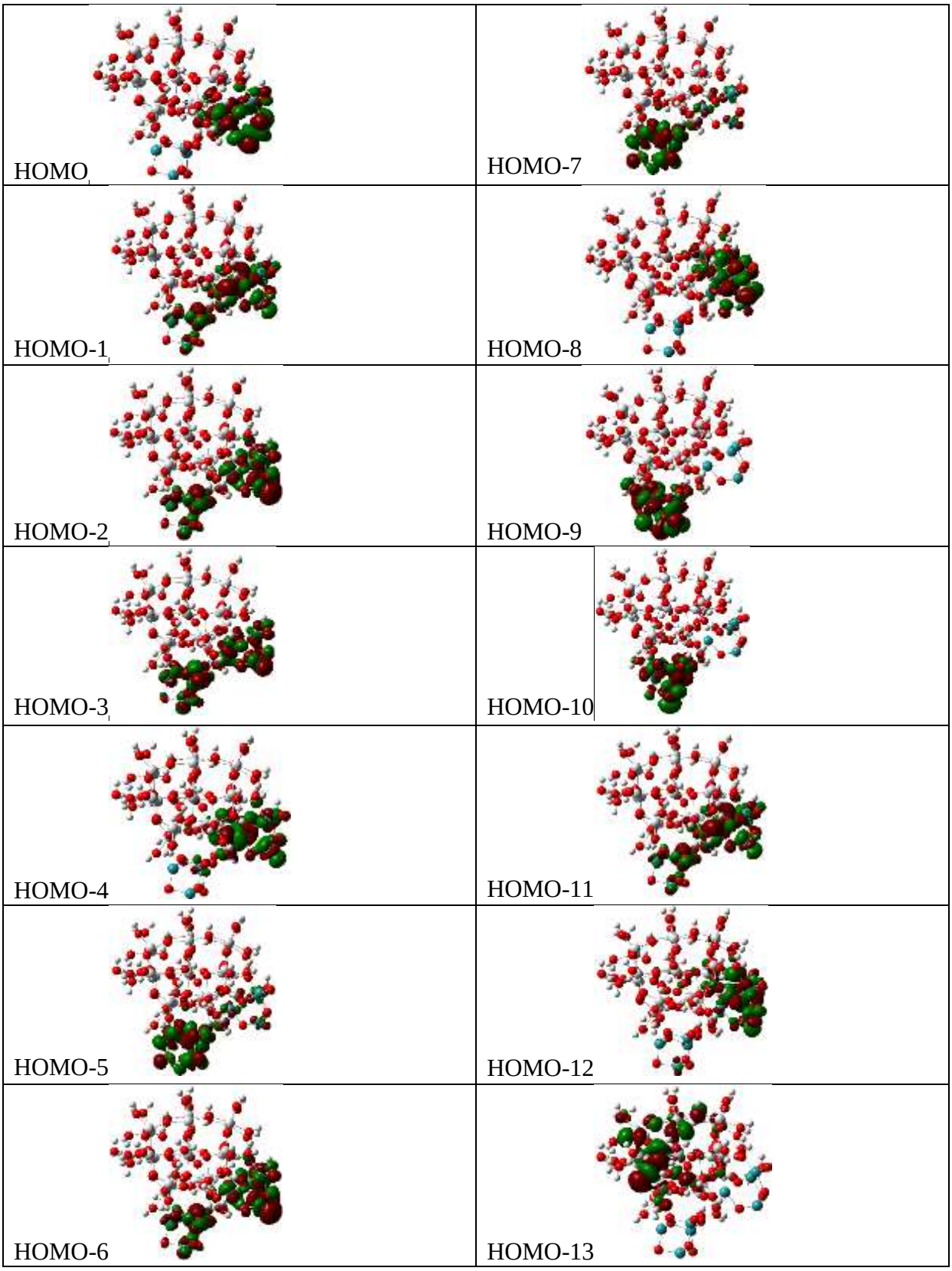

Figure S16: Occupied molecular orbitals (HOMO to HOMO-13) of cluster **f**.

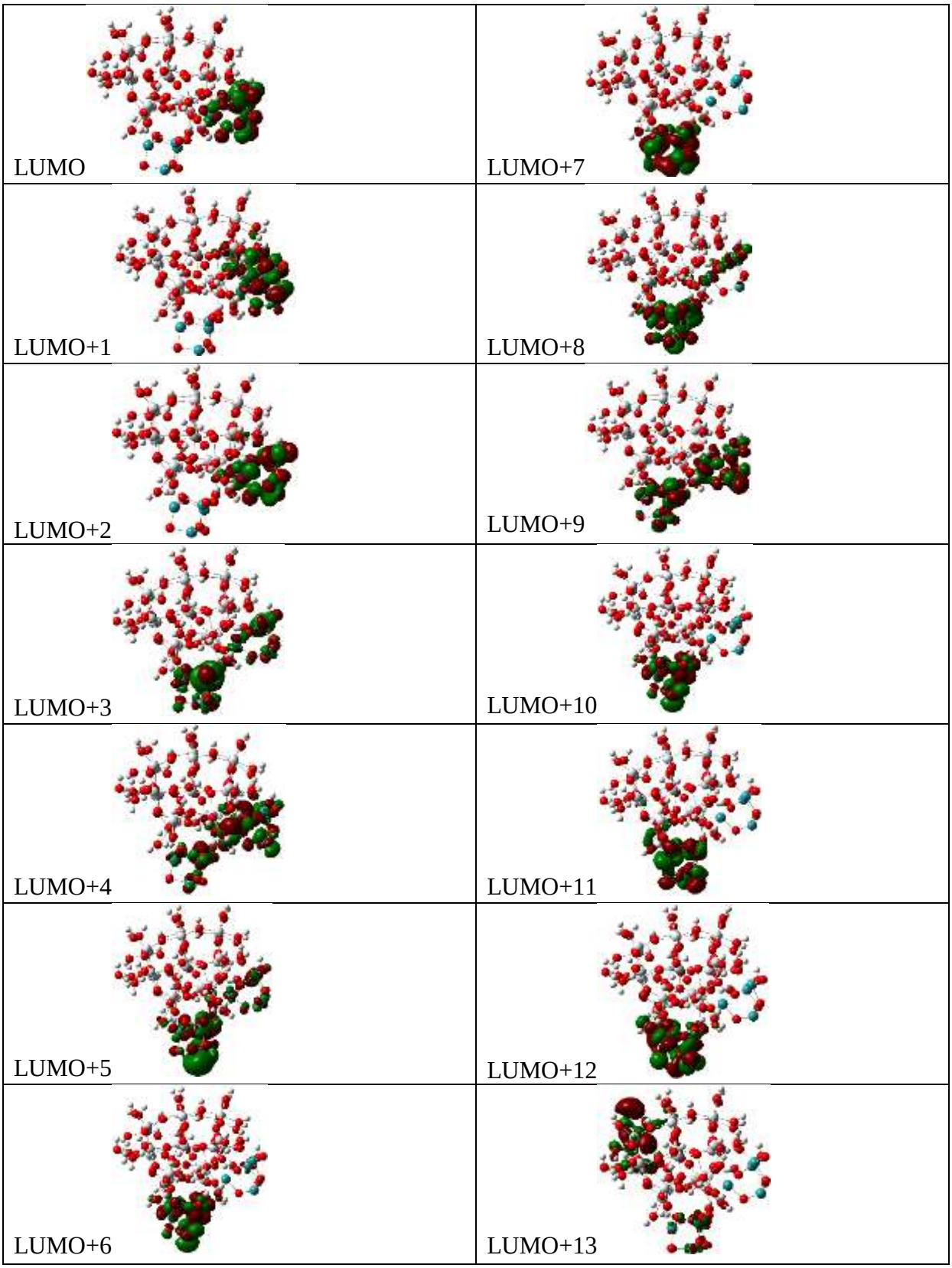

Figure S17: Unoccupied molecular orbitals (LUMO to LUMO+13) of cluster **f**.

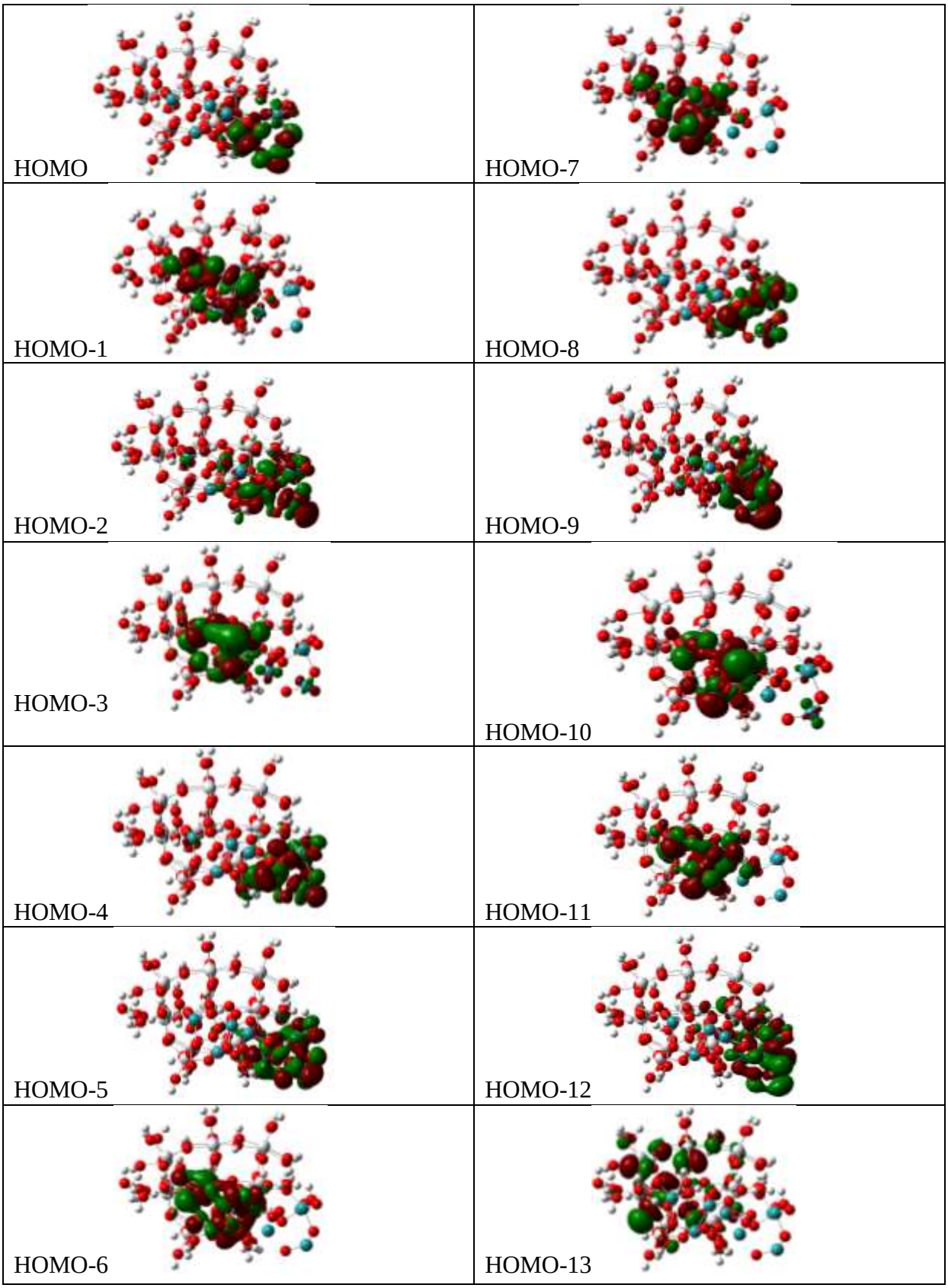

Figure S18: Occupied molecular orbitals (HOMO to HOMO-13) of cluster **g**.

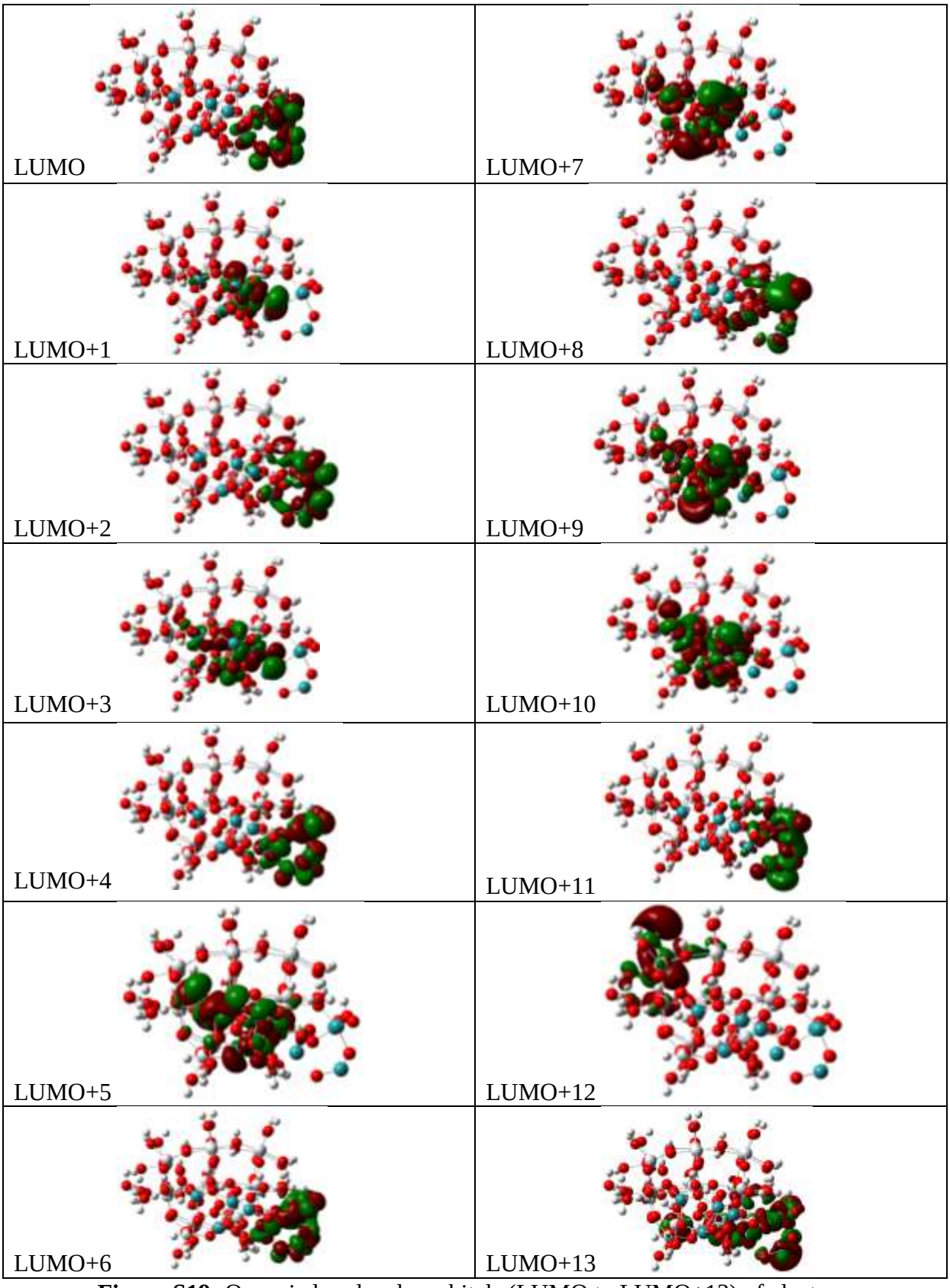

Figure S19: Occupied molecular orbitals (LUMO to LUMO+13) of cluster **g**.